

Resonant Raman-scattering spectroscopy of polydiacetylene films at high pressure

L. X. Zheng,* B. C. Hess,[†] R. E. Benner, and Z. V. Vardeny

*Departments of Physics and Electrical Engineering and the John A. Dixon Laser Institute,
University of Utah, Salt Lake City, Utah 84112*

G. L. Baker

Department of Chemistry, Michigan State University, East Lansing, Michigan 48824

(Received 27 April 1992; revised manuscript received 12 October 1992)

We studied the electronic energies and phonon frequencies of polydiacetylene 4-BCMU thin films at high pressures up to 50 kbar using Raman scattering under preresonant and resonant conditions. Pressure-induced changes in the resonant Raman scattering (RRS) include (1) hardening of the most strongly coupled phonon frequencies, (2) dispersion of the RRS frequencies with the laser excitation ω_L , which shift to lower energies in analogy with the red shift of the absorption band at high pressures, and (3) softening and narrowing of the phonon distribution. These observations are consistent with an increase in the average conjugation length with pressure. Amplitude-mode-model analysis of the RRS data shows that the bare phonon frequencies increase with pressure, but otherwise the one-dimensional Peierls-type relation between the phonons and the electronic gap changes very little with pressure.

I. INTRODUCTION

Recently, π -conjugated polymers have been extensively studied because of their ultrafast response and large nonlinearities attributed to one dimensionality and delocalization of the π electrons along the polymer chains.¹⁻³ The polydiacetylenes (PDA) are particularly promising nonlinear optical materials. They have large third-order optical nonlinearities and can be produced in many different forms including single crystals, solutions, Langmuir-Blodgett films, gels, and low-defect thin films deposited from solution.⁴

Resonant Raman scattering (RRS) is an efficient method for studying disorder in conducting polymers, since the inhomogeneously broadened distribution of phonon frequencies caused by the disorder is selectively probed by changing the excitation photon energy ω_L . We have recently used RRS to study disorder in PDA [poly(4-butoxycarbonyl-methylurethane (4BCMU))] films prepared by spin casting from solution onto sapphire substrates at ambience.⁵ The complete RRS spectrum of PDA 4-BCMU films contains approximately eight resonantly enhanced phonon lines. We found, however, that only the Raman frequencies of the C=C and C≡C stretching vibrations strongly shift with the excitation photon energy ω_L in resonance, $1.9 \text{ eV} < \omega_L < 2.4 \text{ eV}$. This phenomenon is known as phonon dispersion. Phonon-dispersion frequencies of 41 cm^{-1} and 38 cm^{-1} for the C=C and C≡C stretching vibrations, respectively, were observed in the resonant spectral range. Phonon dispersions are explained by the process in which different portions of the inhomogeneously broadened phonon distribution are selectively enhanced with the excitation photon energy in resonance. Two competing models, the conjugation length model⁶⁻⁸ and the amplitude mode model (AM),⁹ which have been recently unified,^{10,11} can explain well the RRS photoselection in conducting polymers.

The conjugation length model^{6,7} is based on the free-electron theory of conjugated molecules introduced by Kuhn for linear systems.⁸ In this theory, the π electrons are treated in a potential, which is a finite constant everywhere on a network defined by the σ bonds of the molecule and infinite elsewhere. Because of bond-length alternation, the π -conjugated polymers, such as polyacetylene become one-dimensional semiconductors. Thus, the energy gap E_0 and vibrational frequency ω of the molecule can be expressed as

$$\begin{aligned} E_0 &= A + \frac{B}{L}, \\ \omega &= C + \frac{D}{L}, \end{aligned} \quad (1)$$

where L is conjugation length of the chain, and A , B , C , and D are constants. Chains with shorter conjugation length have larger electronic gap and higher coupled-phonon frequencies. In this approach, therefore, the inhomogeneity in the polymers is attributed to a distribution of chains with varying lengths of π electron conjugation.⁷

In the AM model,⁹ the skeleton chain (i.e., without π electrons) has a few "bare" normal modes, and the strong coupling of π electrons to these normal modes plus the sensitivity of electronic structure to quasi-one-dimensional structural distortion drive the dimerization. Thus, the total electronic energy of a conjugated molecular chain can be written as the sum

$$E_T = E_\sigma + E_\pi, \quad (2)$$

where E_σ and E_π are the σ - and π -electron energies, respectively. The second derivative of E_T yields the total force constant for the vibrations. The second derivative of E_σ with respect to the normal coordinates yields the force constant for the bare normal models, which determine the bare frequencies in the skeleton chain (i.e., without π electrons).

Since E_π is a function of the carbon-carbon distance, the vibrational modes are coupled to the π electrons, and hence, they respond to the total deviation of the bond length from its equilibrium value. The π electrons tend to reduce the force constant, since the second derivative of E_π is, in general, negative. Thus, in the case of a single-vibration-mode system, the vibration frequency ω is lower than the elastic (or bare) vibration frequency ω_0 ,

$$\omega^2 = \omega_0^2 - (\omega_0^2/K) |E_\pi''|, \quad (3)$$

where $K = d^2E_\sigma/du^2$ is the elastic force constant. The vibrational force constant is thus reduced, with respect to the elastic force constant K , by a factor $\tilde{\lambda}$ given by

$$2\tilde{\lambda} = \omega^2/\omega_0^2 = 1 - |E_\pi''|/K. \quad (4)$$

The dimensionless ‘‘renormalization’’ parameter $\tilde{\lambda}$ is an important parameter in the AM model⁹ and physically provides a measure of the contribution to the force constant of the π electrons. It contains all the effects of electron-phonon, electron-electron, and disorder interaction. In principle, $\tilde{\lambda}$ can be calculated from a model, but in practice it is usually determined by fitting to experimental data. For multimode vibrations, the overall coupling $\tilde{\lambda} = \Sigma \tilde{\lambda}_n$, where $\tilde{\lambda}_n$ is the dimensionless coupling constant for the n th mode, can be expressed as a product rule relation,

$$\prod (\omega_n/\omega_n^0)^2 = 2\tilde{\lambda}. \quad (5)$$

In the presence of the π electrons, the new set of the Raman-active frequencies are determined by the poles of a combined phonon propagator for the normalized modes, $D(\omega)$.

$$D(\omega) = \frac{D_0(\omega)}{1 + (1 - 2\tilde{\lambda})D_0(\omega)}, \quad (6)$$

where $D_0(\omega)$ is ‘‘the bare propagator’’ given by

$$D_0(\omega) = \sum \frac{\tilde{\lambda}_n}{\tilde{\lambda}} \frac{\omega_n^0}{\omega^2 - (\omega_n^0)^2 + i\omega\gamma_n} \quad (7)$$

and γ_n are the inverse lifetimes of the modes. Thus, the bare frequency ω_0 and $\tilde{\lambda}$ can be determined by (5) and $-1/(1 - 2\tilde{\lambda}) = D_0(\omega)$ through a fitting process to the experimental Raman dispersion with ω . In this approach,⁹ the inhomogeneity in both the electron-phonon and electron-electron interaction parameters results in the dispersion of RRS frequencies and a distribution in the π electron gap. In this research, both of these two theoretical models will be used.

It has been shown⁵ that the disorder-induced distributions in the exciton levels in PDA films cause strong dispersion of the C=C and C≡C stretching vibrational frequencies with ω_L in both Stokes and anti-Stokes configurations. Using the AM model and the experimental data of RRS in PDA 4-BCMU films, we have obtained a ‘‘Peierls-type’’ relation for E_g with $E_g \sim \exp(-1/2\tilde{\lambda})$ at ambience. We have also shown⁵ that when the excitation energy is out of resonance at $\omega_L < 1.9$ eV, a very broad Stokes Raman line [fullwidth at half maximum (FWHM)

of about 60 cm^{-1}] for the C=C stretching vibration is obtained; since this line essentially contains all Raman frequencies that are excited at ω_L in resonance and preresonance, it reveals the complete inhomogeneously broadened phonon distribution in the sample.

In order to better understand the properties of polydiacetylene, the changes in the optical absorption spectra and the Raman-scattering spectra of PDA crystals and solutions with pressure have been measured by several groups.^{12–15} It was found that the peak in the absorption spectrum red shifts and modes associated with the vibrations of the polymer backbone harden with increasing pressure.

In this paper, we report studies of resonant Raman scattering of PDA 4-BCMU at high pressure. The experimental method is introduced in Sec. II. The hardening of the vibrational frequencies, the change of their linewidths and line shapes, and the change of the phonon frequency distribution at high pressures are presented in Sec. III. In Sec. IV, the increase of the backbone bare frequencies with pressure is calculated using the AM model. Two competing mechanisms observed at high pressures, including phonon hardening and softening, are also discussed in detail in Sec. IV.

II. EXPERIMENTAL METHOD

Raman-scattering data were recorded in a transmission-scattering geometry. Various excitation lasers were used including HeNe, Ar⁺, Ar⁺-pumped dye (in the Rh6G and DCM dye spectral ranges), frequency-doubled Nd:YAG and Ar⁺-pumped Ti:sapphire. After passing through a plasma line filter (Spex), the laser beam was focused onto the sample using a spherical lens with a focal length of 8 cm to produce a spot size diameter of about $60 \mu\text{m}$ (with excitation at 590 nm). Irradiation levels of the PDA samples were kept below 10^4 W/cm^2 to suppress light-induced defects in the films and to avoid sample damage. The scattered radiation was collected at $f/1.2$ using a camera lens (Nikon) and imaged at $f/7$ using a 35-cm focal length achromatic doublet onto the entrance slit of a triple spectrograph (Spex 1877). The triple spectrograph contained either 300, 600, or 1200 g/mm classically ruled gratings. Optical multichannel detection of the Raman scattered intensity was accomplished using a liquid-nitrogen-cooled CCD (charge-coupled device, Thomson CSF) having an array of 384×576 pixels with dimensions of $23 \times 23 \mu\text{m}$ placed at the exit plane of the spectrograph. For most measurements, the 1200-g/mm gratings were used to obtain a spectral resolution of about 1 cm^{-1} per pixel in the red to visible range. Depending upon excitation wavelength ω_L , Raman spectra were recorded with exposure times ranging from 10 to 200 s for each ω_L in resonance and from 10 to 30 min for each ω_L in nonresonance.

For Raman-scattering measurements at high pressures, the PDA 4-BCMU films were cast from solution on 12- μm -thick Mylar sheets, and small uniform pieces were cut to fit in the gasketed chamber of a Piermarini-Block diamond-anvil cell. We show in the next section that the Mylar had negligible effect on the pressure in the film.

Water was used as the quasihydrostatic pressure medium. The pressures were determined from measurements of the ruby fluorescence line widths and shifts.¹⁶ In our experiment the highest pressure reached was 70 kbar.

III. EXPERIMENTAL RESULTS AND ANALYSIS

The change in optical absorption of PDA films with pressure is shown in Fig. 1(a). We see from Fig. 1(a) that the absorption band red shifts with pressure. The red shift of the absorption band (E_g) with increasing pressure as determined from the extrapolation of the band edge is shown in Fig. 1(b). Up to approximately 35 kbar, a red shift in E_g of about 10 meV/kbar was measured; however, saturation sets in at about 40 kbar [Fig. 1(b)]. The main contribution to the decrease of E_g with pressure is expected to be a solvent effect.¹⁷

RRS is also an efficient tool to probe disorder, the structural changes, and the interchain interaction in π conjugated polymers at high pressures. At high pressure, the C=C and C \equiv C stretching vibrations in PDA 4-BCMU films still show strong RRS dispersion. Typical Stokes RRS spectra of the C=C vibration for various excitations ω_L at a pressure of 21 kbar are shown in Fig. 2. Comparison of the Raman dispersion spectra with

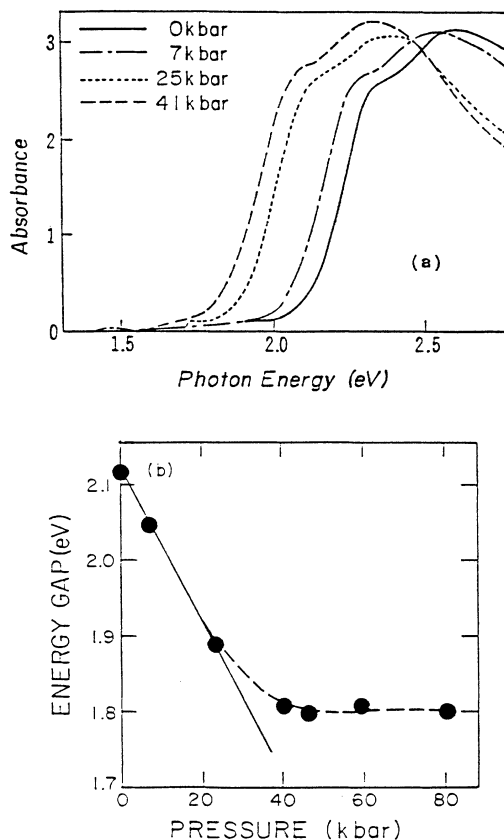


FIG. 1. (a) Optical density of the PDA 4-BCMU film at various pressures. (b) Variation of the energy gap E_g of PDA film extrapolated from (a).

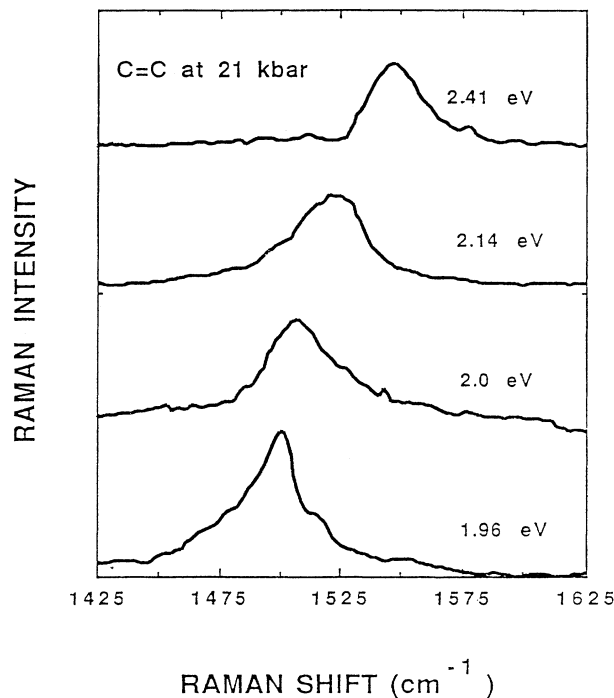


FIG. 2. Raman scattering of C=C stretching vibration at 21 kbar for various excitation photon energies.

those at ambient pressure indicates that the phonon frequencies increase by 18 cm^{-1} irrespective of ω_L and all Raman linewidths broaden by about 7 cm^{-1} at high pressure for ω_L in resonance or for pre-resonant excitation.

Measured phonon dispersion curves for C=C and C \equiv C stretching vibrations similar to the ones shown in Fig. 2 for pressures of 1 bar, 10 kbar, and 42 kbar, respectively, are shown in Figs. 3 and 4. We note that phonon dispersion occurs at each high pressure, but also that the whole dispersion curve blue shifts with increasing pressure.

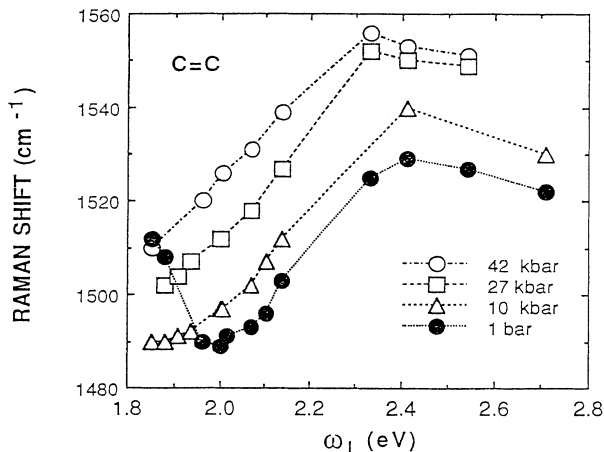


FIG. 3. RRS dispersion with ω_L for the C=C stretching vibration at various pressures.

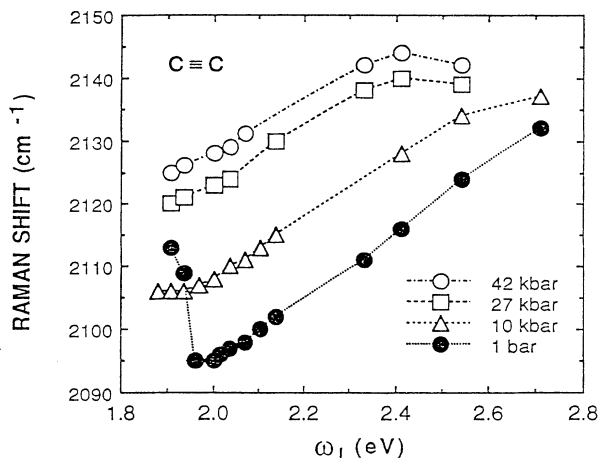


FIG. 4. RRS dispersion with ω_L for the $C\equiv C$ stretching vibration at various pressures.

The disorder-induced dispersion observed at ambience also has a large effect on the Raman spectra at high pressures. The resonance region is approximately the portion of the dispersion curve in which the phonon frequency ω is linear with the laser photon energy ω_L between about 1.9 and 2.3 eV. Since the absorption band red shifts with pressure (Fig. 1), the Raman resonance excitation spectrum also red shifts. On the other hand, the phonons observed at a given excitation wavelength also, generally, harden. These two effects cause the curves in Figs. 3 and 4 to shift with pressure to the upper left, i.e., to higher frequencies and lower photon energies.

Because of this dispersion, the dependence of the Raman spectra on pressure can be quite complicated, superimposing both preresonance and resonance spectra, depending on the relative position of the excitation energy in the red-shifting absorption band. We found that from 580 nm to 620 nm the resonant peak dominates at all pressures, and the peak frequency of the $C=C$ stretching vibration increases linearly with pressure. Figure 5 shows the Raman peak frequency ω as a function of pressure for the $C=C$ stretching vibration excited at $\omega_L = 2$ eV (620 nm). Even though the absorption-band red shift saturates at approximately 30 kbar in our PDA films [Fig. 1(b)], ω increases linearly with pressure up to 46 kbar. Thus, the hardening is independent of the absorption-band movement with pressure. The linear shift in the $C=C$ stretching vibration is $0.9 \text{ cm}^{-1}/\text{kbar}$ when excited at 620, 600, and 580, nm; this gives a Grüneisen mode parameter $\gamma = 1 d\omega/\omega dp$ of 6×10^{-4} kbar for the $C=C$ vibration. For the $C\equiv C$ stretching vibration, on the other hand, the shift with pressure is sublinear at these same wavelengths, giving a Grüneisen mode parameter $\gamma = 5 \times 10^{-4}$ kbar. The hardening is similar to that seen in PDA-PTS (polydiacetylene toluene sulfonate) crystals, but the γ values in PDA-PTS crystals¹⁵ are only 3.3×10^{-4} kbar and 4.5×10^{-4} kbar for $C=C$ and $C\equiv C$ stretching vibrations, respectively. For the $C=C$ stretching vibration of polyacetylene $(CH)_x$,¹⁸ γ is only 2.3×10^{-5} kbar. This comparison shows that solution-cast PDA films are probably more

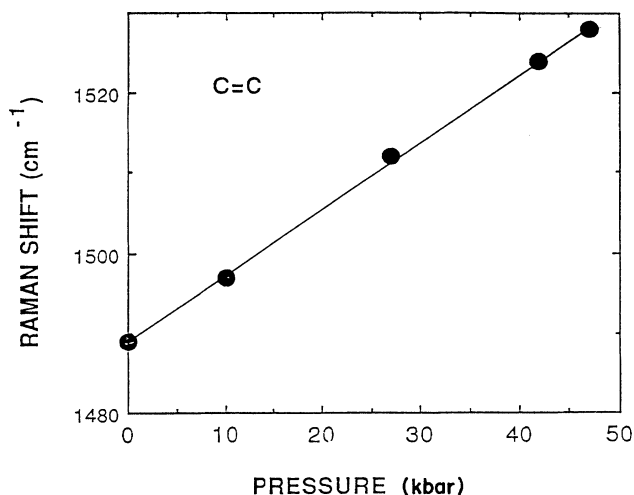


FIG. 5. Pressure dependence of the $C=C$ stretching vibration in RRS at excitation of 620 nm.

sensitive to pressure than PDA-PTS crystal and polycrystalline $(CH)_x$.

The absorption and Raman pressure shifts give us an internal pressure gauge for the film, from which we can conclude that the Mylar substrate has no noticeable effect on the compressibility of the PDA film. In Fig. 1(b) we see that up to 20 kbar the film on Mylar has the same pressure red shift of 10 meV/kbar as observed in *free-standing* PDA 4-BCMU films.¹³ The fact that the resonant Raman lines harden uniformly (linearly) over the *entire* pressure range of our experiments (see Fig. 5) indicates that the Mylar continues to have no effect on the

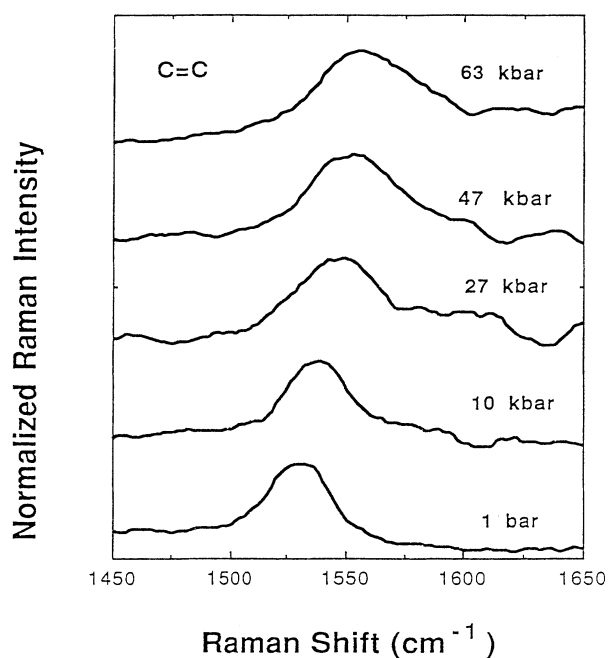


FIG. 6. RRS spectra of the $C=C$ stretching vibration at excitation of 514.5 nm, for various pressures.

properties of the film at higher pressure. Any strain effects of the Mylar on the film appear to be relaxed within a small fraction of the film thickness because of the low shear strength of the disordered polymer 4-BCMU film (i.e., gel).

In Fig. 6 the increase of Raman frequencies and broadening of Raman linewidths with pressure is shown for the C=C stretching vibration at $\omega_L=2.41$ eV, which is above strict resonance leading to phonon dispersion. The pressure dependence of phonon frequencies and linewidths are summarized in Figs. 7(a) and 7(b), respectively. Figure 7(a) shows that the phonon frequencies deviate from a linear increase at approximately 20 kbar and saturate at higher pressures than 40 kbar. The Raman linewidths, on the other hand, increase almost linearly with pressure. We note that at high pressure both the excitation photon energy of 2.41 eV and $\omega_L - \omega$, where ω is the phonon energy are actually away from resonance because the exciton line red shifts at high pressure. For $\omega_L=2.41$ eV, the vibrational frequency and linewidth of the C=C stretching vibration also show the same behavior in RRS. From Fig. 7 and a similar dependence for the C≡C stretching vibration, $d\omega/dP$ values

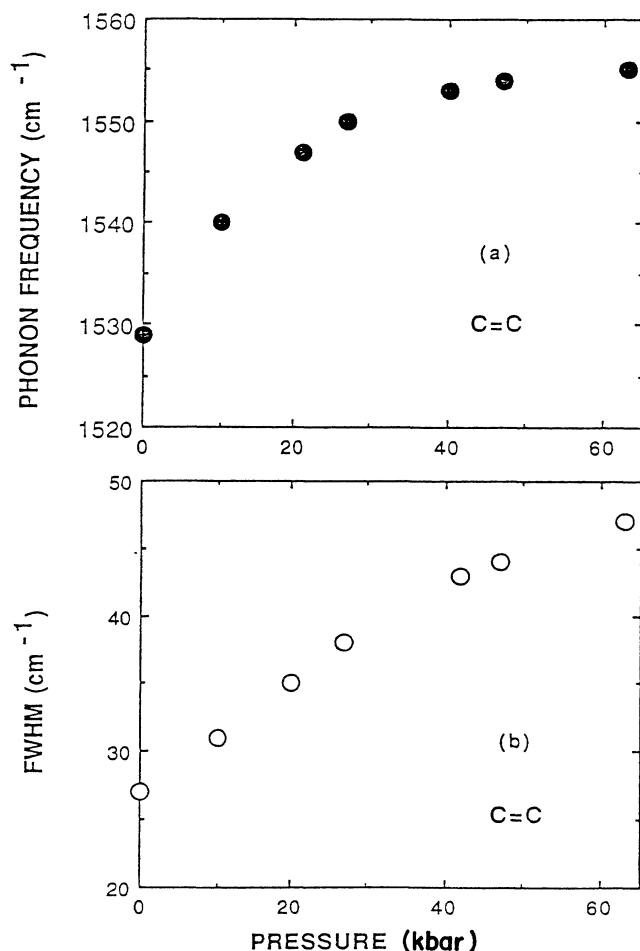


FIG. 7. Pressure dependence of (a) the Raman frequency and (b) the FWHM of the RRS line for the C=C stretching vibration at excitation of 514.5 nm.

for the C=C and C≡C stretching vibrations were calculated to be $0.81 \text{ cm}^{-1} \text{ kbar}$ ($\gamma=5.4 \times 10^{-4} \text{ kbar}$) and $0.92 \text{ cm}^{-1} \text{ kbar}$ ($\gamma=4.4 \times 10^{-4} \text{ kbar}$), respectively.

When the laser excitation was fixed at $\omega_L=1.85$ eV (670 nm) (which is not in resonance at ambience), the Raman-scattering spectrum reveals the entire phonon distribution of PDA films as mentioned in Sec. I. The Raman spectra at various pressures with $\omega_L=1.85$ eV are shown in Fig. 8. The line shape of the Raman lines changes substantially with increasing pressures. The center frequencies of the lines harden, and the spectrum becomes narrower. For ω_L at 1.85 eV, the red shift of the exciton line should be taken into account. Since $\omega_L=1.85$ eV is already in pre-resonance at 30 kbar, Raman-scattering spectra with a single peak structure and a narrow linewidth are observed. Thus, the Raman spectrum at high pressure for $\omega_L=1.85$ eV is no longer dispersion free, explaining the narrow spectrum at 50 kbar.

Since resonant excitation gives the pressure shift of only one group of phonons in the inhomogeneously broadened distribution, we used the nonresonant Raman-scattering technique to measure the effect of pressure on the entire phonon distribution in the sample. Figure 9 shows Raman spectra of the C=C stretching vibration excited at 760 nm (1.65 eV) for 27 kbar and 650 nm (1.88 eV) for 1 bar, for the same sample; these two ω_L were chosen to be equidistant from the band edge at both pressures using Figs. 1(a) and 1(b). Therefore, a direct comparison of the phonon frequency distribution at 1 bar and 27 kbar is possible. Figure 9 shows that the phonon distribution is narrower at 27 kbar, and that the Raman peak has a small net blue shift. This indicates that the

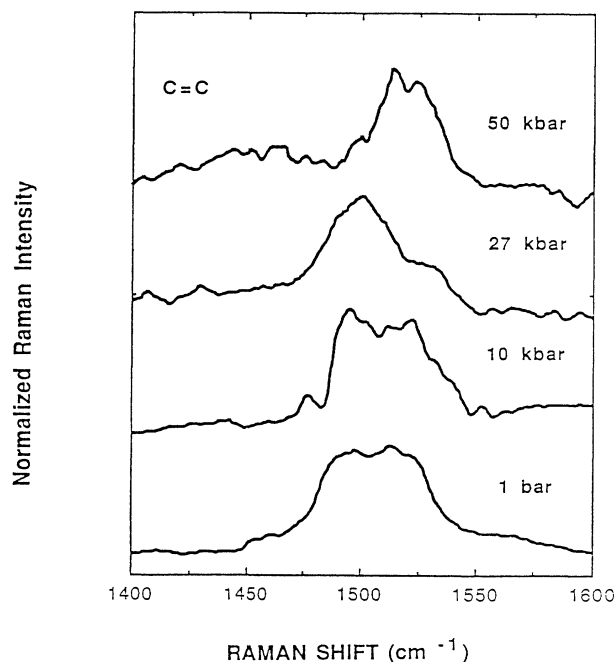


FIG. 8. Raman scattering spectra of the C=C stretching vibration at excitation of 670 nm, for various pressures.

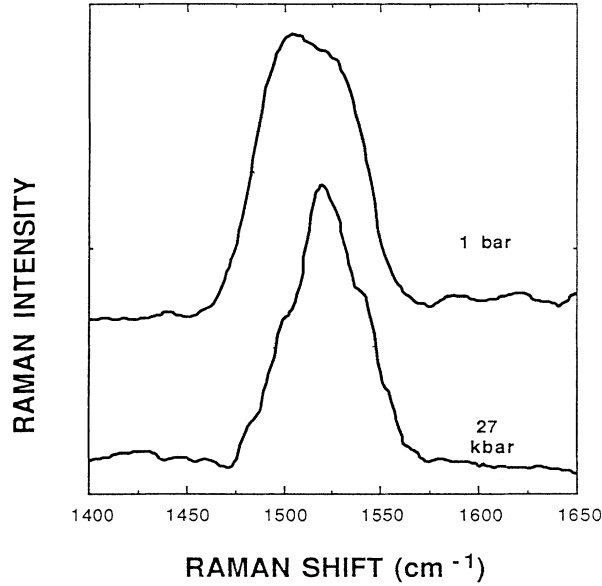


FIG. 9. The whole distribution of the C=C stretching vibrations at 1 bar and 27 kbar, probed at excitations of 650 and 760 nm, respectively. These two excitation wavelengths are chosen to be equidistant from the band edge at both pressures providing equal preresonant conditions.

phonon distribution at high-pressure substantially differs from that at ambience, and the sample appears to be more ordered at high pressure. The relevant mechanisms for this ordering are discussed in the next section.

IV. DISCUSSION

A useful analysis for the RRS dispersion in conducting polymers is provided by the AM model.⁹ A powerful relation is the multiplication rule $\Pi_n(\omega_R^n) \sim 2\tilde{\lambda}$ where ω_R^n are the Raman frequencies of all A_g modes that are resonantly enhanced at ω_L and $\tilde{\lambda}(\omega_L)$ are the renormalization parameters for the AM frequencies at ω_L . The AM model analysis at ambient pressure showed⁵ that the disorder distribution in PDA films can be described by a “Peierls-type” relation.

Since the phonon-dispersion curves at pressures of 10, 27, and 42 kbar were obtained in the full resonance region, the disorder can be analyzed at those pressures using the AM model. Using the multiplication rule, we plot $\Pi_i(\omega_p^i/\omega_s^i)^2$ vs $\ln(\omega_L)$, where ω_p^i and ω_s^i are all eight RRS frequencies at $\omega_L^p = \omega_x$ (ω_x is the exciton resonance) and at ω_L^s , respectively. Figure 10 shows the results at 42 kbar. We can readily see that the RRS frequencies ratio at high pressures can be also fit by $-\ln(\omega_L)$, and we obtain the following relations:

$$\tilde{\lambda}_p/\tilde{\lambda}(\omega_L) = 1.45 - 0.58 \ln(\omega_L),$$

or (8)

$$\tilde{\lambda}_p/\tilde{\lambda}(\omega_L) = 1 - 0.58 \ln(\omega_L/\omega_x),$$

where $\tilde{\lambda}_p$ is $\tilde{\lambda}$ at ω_x . In order to find $\tilde{\lambda}$ and ω_0^n (the bare frequencies), a complete fit to the RRS data using the

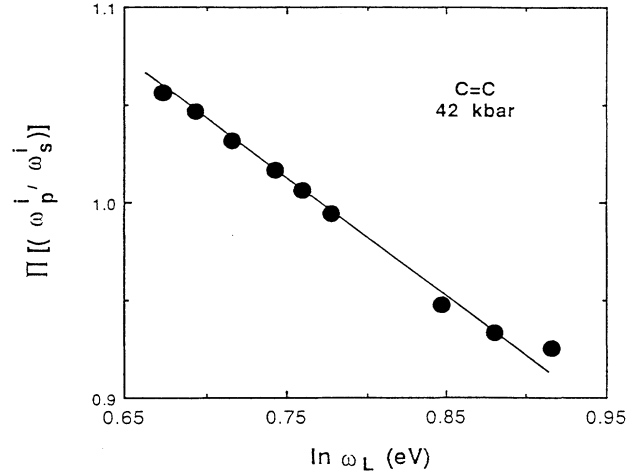


FIG. 10. The multiplication ratio $\Pi_i(\omega_p^i)^2/\Pi_i(\omega_s^i)^2$ ($\sim \tilde{\lambda}$) for all nine RRS vibrations in PDA films at 42 kbar vs $\ln(\omega_L)$; p denotes excitation at $\omega_L = \omega_x$ (the exciton band) and s stands for any ω_L . The straight line is a theoretical fit to the data using a “Peierls-type” relation.

AM model is necessary.⁹ For this fit we used the Raman frequencies obtained at the laser excitation frequencies shown in Fig. 10, a nonlinear least square fitting program, and the following equations:

$$\frac{1}{2\tilde{\lambda}} = A - \ln(\omega_L), \quad (9)$$

$$\frac{1}{2\tilde{\lambda}} = \sum \frac{\tilde{\lambda}_n}{\tilde{\lambda}} \frac{\omega_n^0}{\omega_n^2 - (\omega_n^0)^2}, \quad n = 1, 2, 3 \quad (10)$$

$$\sum \frac{\tilde{\lambda}_n}{\tilde{\lambda}} = 1, \quad (11)$$

where $n = 1$ stands for the C—C vibrations; ω is an average value of six Raman frequencies associated with C—C stretching vibrations; $n = 2$ and 3 stand for the C=C and C≡C stretching vibrations, respectively. The best fitting parameters at ambience and at various pressures are given in Table I.

The “Peierls-type” relation, $E_g = 4E_C \exp(-1/2\tilde{\lambda})$ still holds at high pressures, indicating that the dispersion is described by a Peierls-type relation at all pressures.¹⁸ We also note from Table I that neither E_C nor the mode-coupling constants $\tilde{\lambda}_n$ change noticeably with pressure. We find, however, that the dominant effect of pressure is to increase the C=C and C≡C bare frequencies. Although our fit gives a sublinear shift in the bare frequencies, we can still calculate the overall bare mode Grüneisen parameters. They are 7.6×10^{-4} kbar and 6.0×10^{-4} kbar for the bare C=C and C≡C modes, respectively. The γ values obtained from the bare frequencies are obviously larger than those measured at the excitation of 514.5 nm and 620 nm (Fig. 5). This is due to the fact that K_σ increases with pressure, whereas K_π (E_π'') decreases with pressure, and the bare frequencies show only the effect of K_σ , whereas the measured frequencies show the effects of both K_σ and K_π .

TABLE I. The fitting parameters of the AM model (Ref. 9) at various pressures. The bare frequencies ω_0 are given in cm^{-1} ; A is given in eV.

	Atmospheric pressure	10 kbar	25 kbar	42 kbar
Peierls relation parameter A	2.526	2.484	2.468	2.508
ω_0 (C—C)	1120	1123	1126	1127
ω_0 (C=C)	1693	1708	1727	1738
ω_0 (C≡C)	2360	2378	2396	2406
$\tilde{\lambda}_1/\tilde{\lambda}$ (C—C)	0.1	0.071	0.059	0.055
$\tilde{\lambda}_2/\tilde{\lambda}$ (C=C)	0.3	0.305	0.305	0.3
$\tilde{\lambda}_3/\tilde{\lambda}$ (C≡C)	0.6	0.624	0.636	0.645

In principle, the increase in phonon frequencies results from a decrease in bond length and, consequently, an increase in the backbone force constant K_σ at high pressures which, in turn, causes phonon hardening.¹⁹ This effect alone, however, cannot explain all the experimental results at high pressures. Since resonant excitation gives the pressure shift of only one group of phonons in the inhomogeneously broadened distribution, we used preresonant Raman scattering to measure the effect of pressure on the entire distribution of phonons in the samples, as shown in Fig. 9. The phonon distribution is narrower at 27 kbar. The peak has a small net negative shift, suggesting that some process $(d\omega/dP)_s$ softens the phonon hardening $(d\omega/dP)_h$ discussed above. Because there is only a slight positive shift, we conclude that $(d\omega/dP)_s \approx (d\omega/dP)_h$.

In the “solvent” density model,¹⁷ the absorption band red shifts, while the phonon distribution remains unchanged. Neglecting phonon hardening, the model would predict that the dispersion curves in Figs. 3 and 4 shift only to the left with pressure, to lower photon energies. At a fixed excitation energy, this gives an increase in $\omega_{\text{C=C}}$ with pressure of $(d\omega/dP) = (d\omega/dE)(dE/dP) \approx (120 \text{ cm}^{-1}/\text{eV})(0.10 \text{ eV/kbar}) = 1.2 \text{ cm}^{-1}/\text{kbar}$, larger than the $0.9 \text{ cm}^{-1}/\text{kbar}$ observed in our measurements; hardening of the bare phonons with pressure (which must occur to some degree) would make the model prediction even worse. In addition, the frequency shift at fixed excitation energy should saturate with dE/dP at about 30 kbar, which does not occur. While the solvent effect appears to dominate the absorption red shift of 4-BCMU in a good solvent,¹⁷ it alone does not appear to describe the effects we see in the solid films.

Any successful model of the pressure effects reported here must include a mechanism that softens the phonon frequencies in parallel with the electronic band red shift. Since the resonance dispersion proves that the phonons and electron energies can shift together, a natural explanation of the pressure effect could be that pressure shifts the distribution $G(\tilde{\lambda})$ of the effective electron-phonon coupling constants $\tilde{\lambda}$, changing both the phonon and electron distribution of energies. Since pressure does not appear to change the functional relations $\omega(\tilde{\lambda})$ (except for hardening), the phonon-softening mentioned above must occur in the distribution $G(\tilde{\lambda})$.

The strong interaction between the electronic structure

and backbone conformation is a fundamental feature of the π -conjugated polymers. Although conformational transitions are commonly observed in polymer solutions, PDA is unique because of the sensitivity of the electronic properties to the backbone conformation. This sensitivity to conformation originates from the conjugated structure of the PDA backbone [$=RC-C\equiv C-CR=$]. Since π -electronic conjugation requires a planar structure, conformational disorder limits conjugation by disrupting planarity to produce a distribution of various “conjugation lengths” on the individual chains. In other words, there are conjugation-breaking defects on the backbone. These defects cause the individual chains to become twisted rather than planar. It has been proposed^{20,21} that every defect corresponds to a rotation of a P_z orbital about the single bond on the backbone. A simple rotation of $\pi/2$ about the σ bonds (single bonds) between adjacent planes is capable of totally breaking the conjugation, separating the polymer chain into an electronically independent “submolecular” electronic system. Specifically, the energy scale for rotations around the carbon-carbon single bonds is comparable to the thermal energies. Consequently, a considerable number of such rotations can be present even at room temperature. In this way, conformational defects create disorder in the electronic structure and, consequently, in the vibrational frequencies. Thus, the average conjugation length L decreases as the number of rotational defects increases.

Pressure cannot change the actual chain length (end-to-end length) but can change the conjugation length L , where L is the length of the planar segment of the chain. High pressure increases the chain planarity by reducing the out-of-plane rotations, causing the conjugation length L to increase and resulting in a decrease of the phonon frequencies. We propose that this is the origin of the phonon softening with pressure causing both distributions $G(\omega)$ and $G(E_g)$ to shift to lower energies and leading to pressure-induced order. The saturation of the red shift of E_g is probably due to topological disorder that cannot be “pressed out.”¹⁴ The narrowing of $G(\tilde{\lambda})$ seen in Fig. 9 is also consistent with an increase in sample order with pressure. We can test this model for consistency. If both the red shift in E_g and the softening in $G(\tilde{\lambda})$ are due to increasing N (the number of π electrons in the chain), where $L = NR$, and R is the length of carbon-carbon bonds, we then expect the following relation to

hold for the softening of the C=C stretching vibration:

$$(d\omega/dP)_s = (d\omega/dN)(dN/dE)(dE/dP) = B/A(dE/dP), \quad (12)$$

where $E_g(N) = E + A/N$ and $\omega_{C=C}(N) = \omega + B/N$, $A = 4.1$ eV and $B \sim 300\text{--}400$ cm⁻¹.²² In our measurements $dE/dP = 0.01$ eV/kbar and we find $(d\omega/dP)_s = 0.7\text{--}1$ cm⁻¹/kbar for the C=C stretching vibration. When we compare this value to the hardening $(d\omega/dP)_h = 0.9$ cm⁻¹/kbar, which we measured for the C=C stretching vibration at resonant excitation, we see that indeed $(d\omega/dP)_s \sim (d\omega/dP)_h$ as is evident from Fig. 9.

These two effects, (1) changes in $G(\tilde{\lambda})$ that shift the dispersion curves along the line of ω vs E and (2) phonon frequency hardening that shifts the curves $\tilde{\lambda}(P)$ directly upward can accurately describe the pressure changes on the lower-energy side of the dispersion curve. We see from Fig. 3 that the highest-energy part of the linear resonance region does not shift much to lower energies with pressure, probably from short chains or exceptionally twisted chains, which cannot be straightened by pressure.

In summary, we have observed phonon dispersion, hardening of phonon frequencies and change in Raman

linewidth at high pressures in PDA 4-BCMU films. Evidence of pressure-induced order in the films has been obtained by comparing the phonon distribution at ambient pressure with that at high pressure. The bare frequencies of the backbone have been calculated using RRS data and the AM model. The increase of the bare frequencies with pressure is larger than that measured under resonance conditions. At high pressures, there exist two competing mechanisms: (1) hardening caused by an increase in the bare force constant and (2) softening caused by the conformational change. The latter causes the average conjugation length N to increase. The peak of the distribution $G(N)$ shifts to longer N , causing the distribution $G(\omega)$ and $G(E_g)$ to shift to lower energies. This plausible explanation is in agreement with our experimental results.

ACKNOWLEDGMENTS

We thank Professor J. D. Barnett of Brigham Young University for his generous help with the pressure cell. The work at the University of Utah was partially supported by the U.S. Department of Energy Grant No. DE-FG02-89 ER 4509 and by the Free Electron Laser Program at the John A. Dixon Laser Institute at the University of Utah.

*Present address: Department of Chemical Engineering, LSU, Baton Rouge, LA 70803.

†Present address: Physics Department, California State University, Fresno, CA 93740.

¹A. J. Heeger, J. Orenstein, and D. R. Ulrich, in *Materials Nonlinear Optical Properties of Polymers*, Res. Soc. Symp. Proc. No. 109 (Material Research Society, Pittsburgh, 1988).

²P. N. Prasad and D. R. Ulrich, *Nonlinear Optical and Electroactive Polymers* (Plenum, New York, 1988).

³J. Messier, F. Kajzar, P. Prasad, and D. Ulrich, *Nonlinear Optical Effects in Organic Polymers* (Kluwer Academic, The Netherlands, 1989).

⁴D. N. Batchelder, in *Polydiacetylene*, edited by D. Bloor and R. R. Chance (Nijhitt, Doedrecht, 1985).

⁵L. X. Zheng, R. E. Benner, Z. Vardeny, and G. L. Baker, *Phys. Rev. B* **42**, 3235 (1990).

⁶H. Kuzmany, *Pure Appl. Chem.* **57**, 235 (1985).

⁷E. Mulazzi, G. P. Brivio, E. Faulques, and S. Lefrant, *Solid State Commun.* **46**, 851 (1983); G. P. Brivio and E. Mulazzi, *Chem. Phys. Lett.* **95**, 555 (1983).

⁸H. Kuhn, *J. Chem. Phys.* **17**, 1198 (1949).

⁹E. Ehrenfreund, Z. Vardeny, O. Brafman, and B. Horovitz, *Phys. Rev. B* **36**, 1535 (1987).

¹⁰C. Castiglioni, J. T. Lopez Navarrite, G. Zerbi, and M. Gussoni, *Solid State Commun.* **65**, 625 (1988); **74**, 199 (1990).

¹¹J. Kürti and H. Kuzmany, *Phys. Rev. B* **44**, 597 (1991); J.

Synth. Metals **50**, 665 (1992).

¹²R. J. Lacey, D. N. Batchelder, and G. D. Pitt, *J. Phys. C* **17**, 4539 (1984).

¹³B. F. Variano, C. J. Sandoff, and G. L. Baker, *Macromolecules* **24**, 4376 (1991).

¹⁴B. C. Hess, G. S. Kanner, Z. V. Vardeny, and G. L. Baker, *Phys. Rev. Lett.* **66**, 2364 (1991).

¹⁵M. Hangyo, K. Itakura, S. Nakashima, A. Mitsuishi, H. Matsuda, H. Nakanishi, M. Kato, and T. Kurata, *Solid State Commun.* **60**, 739 (1986).

¹⁶G. J. Piermarini, S. Block, and J. D. Barnett, *J. Appl. Phys.* **44**, 5377 (1973).

¹⁷J. P. Aime, H. E. King, M. W. Kim, and R. R. Chance, *Synth. Met.* **41-43**, 225 (1991).

¹⁸Y. Yacoby and S. Roth, *Solid State Commun.* **56**, 719 (1985).

¹⁹H. E. Schaffer, R. R. Chance, R. J. Silbey, K. Knoll, and R. R. Schrock, in *Conjugated Polymeric Materials*, edited by J. L. Bredas and R. R. Chance (Kluwer Academic, Dordrecht, 1990), p. 365; *J. Chem. Phys.* **94**, 4161 (1991).

²⁰R. H. Baughman and R. R. Chance, *J. Appl. Phys.* **47**, 4295 (1976).

²¹V. Dobrosavljevic and R. M. Strat, *Phys. Rev. B* **35**, 2781 (1987).

²²M. L. Shand, R. R. Chance, M. LePostollec, and M. Schott, *Phys. Rev. B* **25**, 4431 (1982).